Supporting Information

SEPARATIONS-ENCODED MICROPARTICLES FOR SINGLE-CELL WESTERN BLOTTING

Burcu Gumuscu, Amy E. Herr

Quantitative microparticle analysis of ER protein isoforms from single cells

Estrogen receptor, ER, is the main contributor to the development of hormone resistance against the therapy in *circa* 70% of breast tumors.[28] Particularly, truncated (ERα46) estrogen receptor isoform is reported to enhance hormone therapy responses by inhibiting the expression of full-length (ERα66) estrogen receptor isoform.[29] The relation between cell confluency and ERα expression in hormone-sensitive cell lines has remained unclear, although this finding may suggest new strategies in therapies. Elucidating mechanisms of confluency-dependent expression of these isoforms requires quantitative measurement of ERα isoforms. We hypothesized that cell confluency level would impact expression levels of ERα46 protein in estrogen-sensitive cells, while no expression would be detected in estrogen resistant and non-expressing cell lines. We used separations-encoded microparticles to address the confluency-dependence of ERα46 and ERα66 expression levels in estrogen sensitive (MCF 7) over 14 days.

We performed slab gel Western blotting assay to validate the microparticle assay results (Figure S5B and Figure S5C). A similar trend in ERα isoform expression levels was observed in slab gel Western analysis, except that no expression could be detected on day 3 of MCF 7 cells unlike microparticle analysis results. We did not observe any detectable signal from ERα isoforms expressed in MDA MB 231 in slab gel Westerns, although microparticles reported 6, 12, 20 cells expressing ERα46 on days 3, 5, and 7, respectively (Figure S7) (n_{total} = 38). We did not observe any ERα isoform signal in HEK 293 cells as shown in Figure S7. Slab gel Western blot analysis confirmed our major finding on ERα expression level changes in MCF 7 cells using microparticle assay, which provided more insight into isoform expression in cell subpopulations.

Characterization of the electric field distribution in microparticle assay

A uniform electric field distribution is compulsory for maintaining repeatable and comparable protein separation in microparticle arrays. In a typical workflow, we apply an electric field across the microparticle array to draw proteins through the microwell wall into the central region of microparticles. The uniformity of the field can be ensured by immersing the unidirectionally placed microparticles on top of a silanized glass plate in a conductive buffer where two parallel platinum electrodes are placed in to apply the electric field. We characterized the uniformity of electric field using two approaches: (1) we simulated electric field distribution in the assay, (2) we tracked the peak position displacement of β-tubulin (50kDa) and GAPDH (35kDa) proteins as a function of time in microparticles placed on a glass slide. Firstly, the electric potential in the microparticle assay was found to be uniform and unaltered between the electrodes according to numerical simulations (Figure S8). This was an expected outcome because polyacrylamide gel must not lead to a discontinued conductivity along the separation axis as long as soaked in the buffer solution during electrophoresis.[38] Simulation result was also confirmed by electrophoresis of β-tubulin and GAPDH proteins obtained from U251 cells (Figure S4). We also tested electrophoretic mobility of two proteins (β-tubulin and GAPDH) on non-silanized glass slides, as it is known that silanization process does not always result in a uniform monolayer of silane groups on the glass slide.[16] Comparison of measured mobilities shown in Figure S4 suggest that silanization state does not have a statistically significant impact on the electrophoretic mobility of the proteins (two sample t-test, p = 0.0001, $n_{silanized\ glass}$ = 20, $n_{non\text{-}silanized\ glass}$ = 20).

Cell-occupancy dependent fluorescence signal changes in separations-encoded microparticles

We compared the antibody fluorescence intensities in multiple-cell occupancy microwells and single-cell occupancy microwells at the central region of microparticles. The mean antibody fluorescence intensity from two-cell occupancy microparticles was ~5.5 times higher than that of single-cell occupancy microparticles (CV = 0.28, n = 10 microwells). The intensity was not doubled (therefore not linear) in two-cell occupancy microparticles due to the cell-size related bias. This result is in accordance with our previous findings.[16]

Characterization of the fluorescent signal intensity distribution

As we discussed in the manuscript, shrinking effect led to increase of the fluorescence signal as the equal number of fluorescence molecules were packed in a smaller volume after dehydration. Interestingly, we observed significantly higher signal at the edges of the central region of separations-encoded microparticles. The edge effect was observed 2.35x higher in hydrated/not probed particles, 5.35x higher in dehydrated particles, 8.11x higher in hydrated particles (Figure S5C). We attribute this occurrence to hydrogel pore size formation at the outer boundaries during polymerization. Polymerization reaction rate is slower at the edges because of the higher oxygen concentrations (oxygen diffuses in the particles passing through the edges first).[39] Reduced reaction rate leads to formation of larger pores, in which fluorescent molecule concentration can be higher.[40] The edge effect did not interfere with the of protein measurements since the background intensity in the central region of the particles was uniformly distributed.

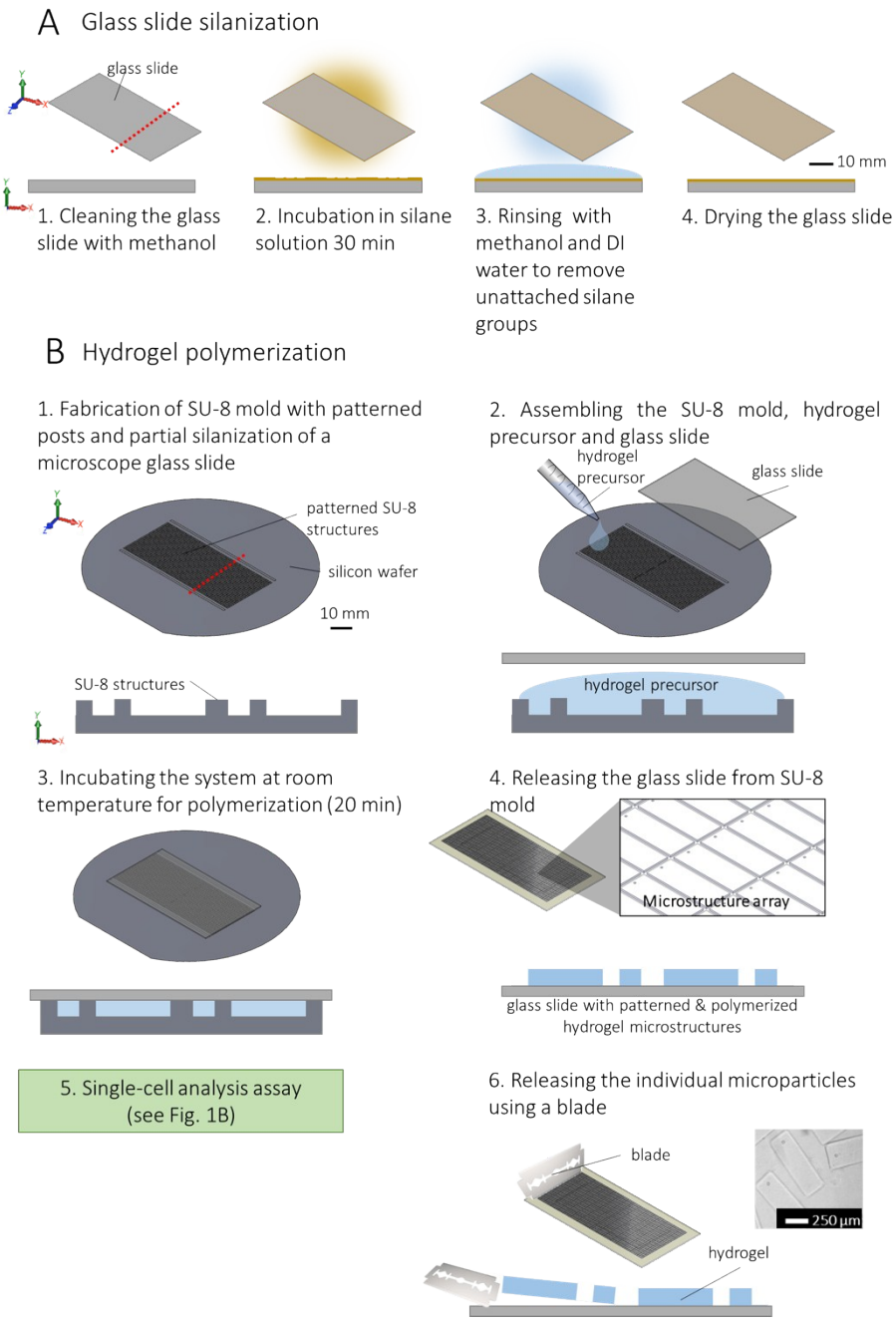

Figure S1. Conceptual description of the workflow of separations-encoded microparticle fabrication. **(A)** A microscope slide is silanized to attach microparticle array on the glass. **(B)** Silanization process is followed by polyacrylamide gel synthesis based on chemical polymerization. Hydrogel precursor is sandwiched between the silanized microscope slide and a silicon wafer with SU-8 posts. After releasing the microscope slide with microparticle patterns from the silicon wafer, single-cell analysis is employed. Individual microparticles can be released from the microscope slide using a razor blade.

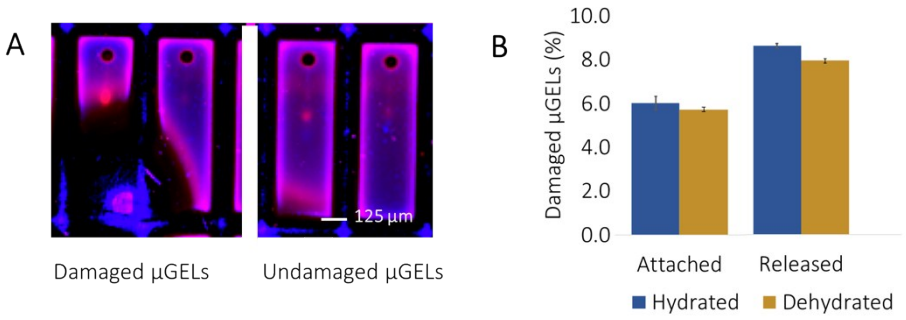

Figure S2. Damage analysis in microparticles. **(A)** False-color fluorescence image of damaged and undamaged microparticles. **(B)** Bar graph shows the percentage of damaged microparticles at hydrated and dehydrated states after and before releasing, $p < 0.0001$ (two sample t-test), n = 2483 microparticles.

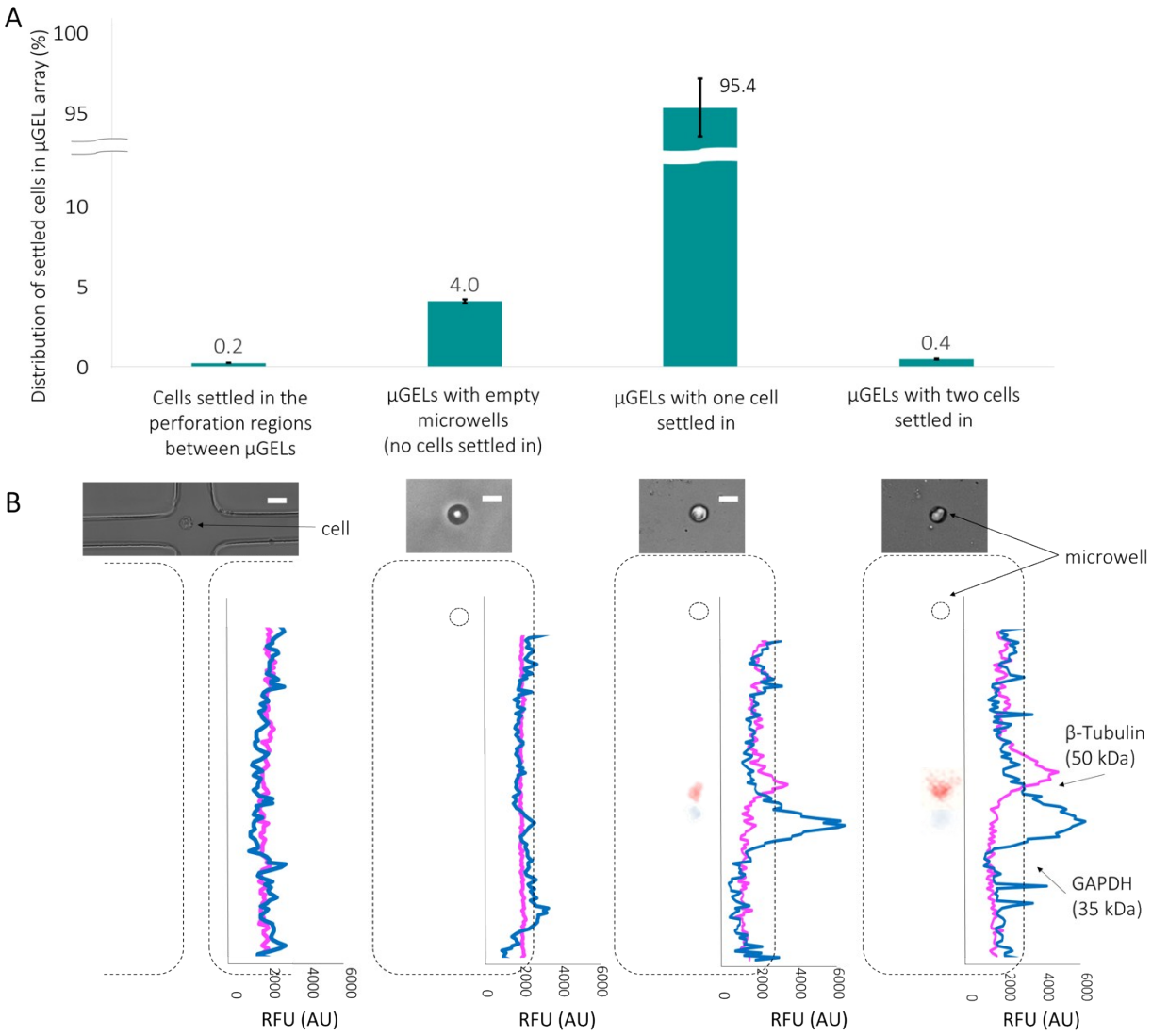

Figure S3. Characterization of cell settling in the microparticle array. **(A)** Bar graph summarizes the distribution of settled cells in microwells (n = 3 devices with 3500 units each). **(B)** Bright field images (top) and fluorescence intensity graphs (bottom) of microparticles. Separation of β-Tubulin and GAPDH proteins are shown and the mean antibody fluorescence intensity from two-cell occupancy microparticles was ~5.5x higher than that of single-cell occupancy microparticles (CV = 0.28, n = 10 wells). The intensity was not doubled (not linear) in two-cell occupancy microparticles due to the cell-size related bias.

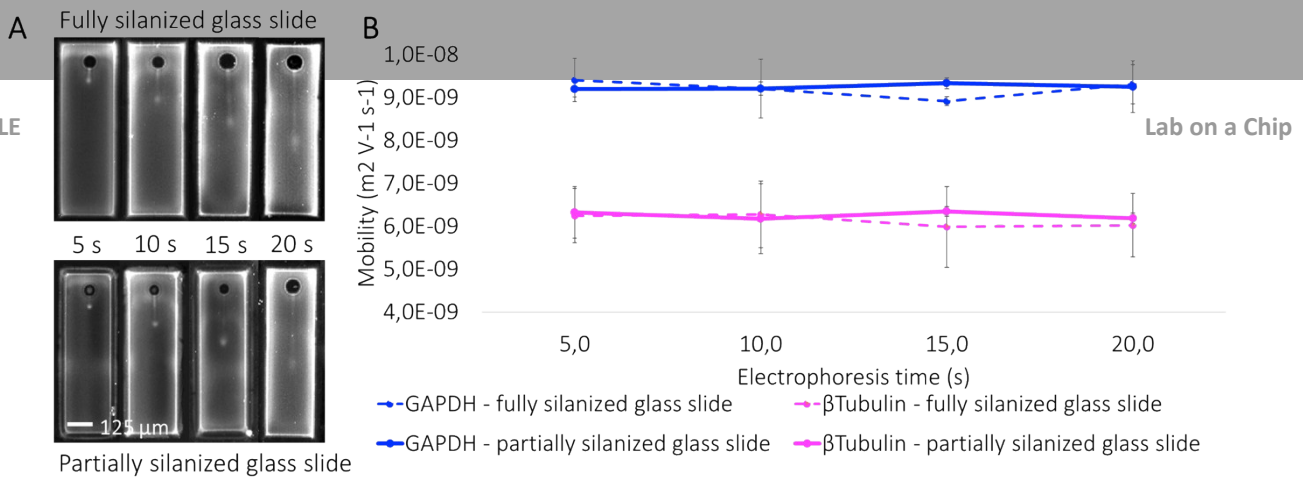

Figure S4. Mobility measurements for β-Tubulin and GAPDH proteins are performed in 8%T 2.6%C polyacrylamide gel microparticles fabricated on partially and fully silanized glass slides. **(A)** Montage of fluorescence micrographs of β-Tubulin at different electrophoresis times on partially and fully silanized glass slides. **(B)** Changes in β-Tubulin (50 kDa) and GAPDH (35 kDa) mobilities in microparticles attached on partially and fully silanized glass slides, n_{total} = 40 microparticles.

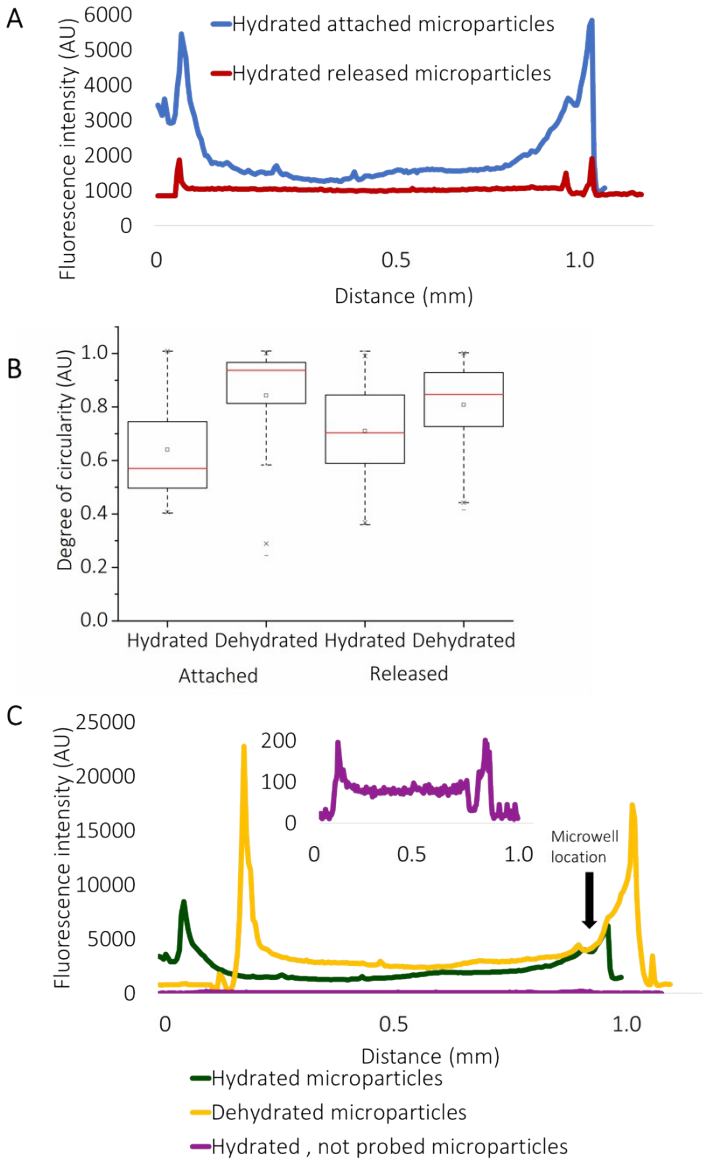

Figure S5. Comparison of fluorescence intensities in microparticles **(A)** Background intensity reduction in released microparticles suggests the geometry-enhanced mass transport during antibody probing and washout steps. **(B)** Characterization of degree of microwell circularity changes in combinations of hydrated, dehydrated, attached, and released states. Surface area normalized to attached hydrated condition is shown in the box plot, $p < 0.00001$ between all groups, $n_{total} = 5090$. **(C)** Fluorescence intensity graph shows signal intensity changes in hydrated/probed, hydrated/not probed, dehydrated/probed microparticles The inset shows a close-up intensity profile of hydrated/not probed microparticles.

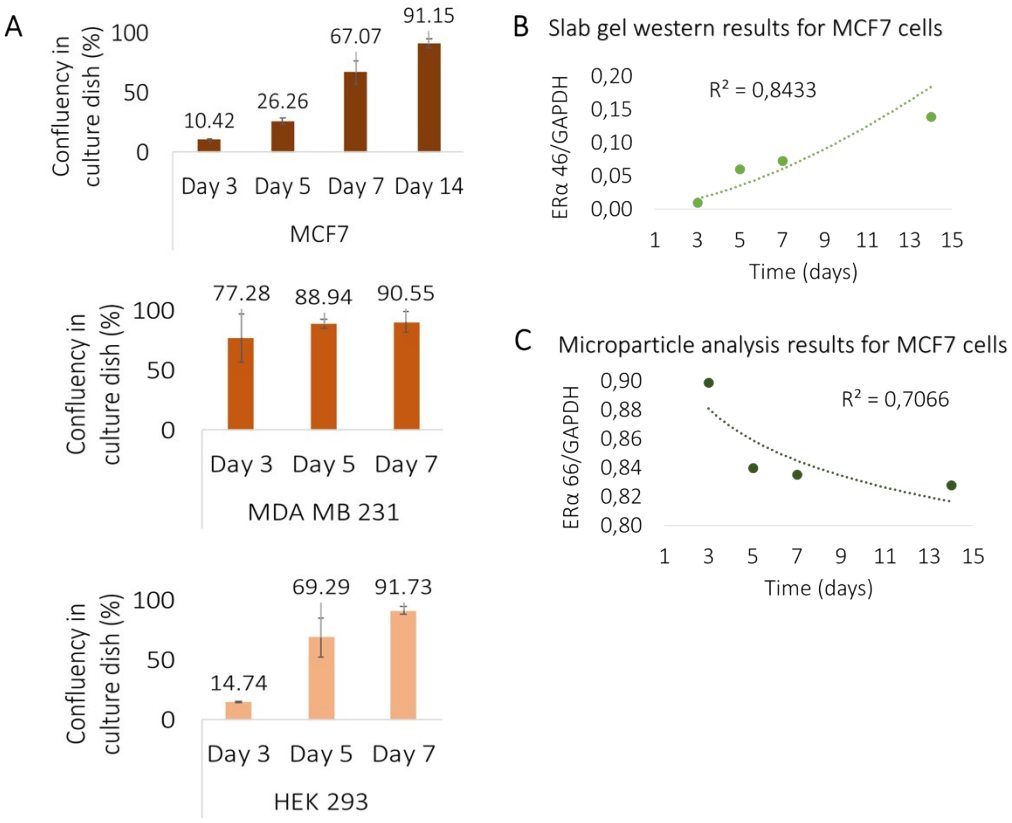

Figure S6. Cell confluency level changes in three cell lines and change of ERα isoform expression over confluency of MCF 7 cells in slab gel westerns. **(A)** The bar graph shows the confluency levels of estrogen sensitive (MCF 7) and resistant (MDA MB 231) breast cancer cell lines as well as HEK 293 cells over 7 and 14 days. MDA MB 231 and HEK 293 cells reached > 90% confluency after 7 days of cell culture. Slab gel western blots (15 mg protein) were performed to confirm microparticle assay results. The scatter graph of **(B)** ERα46 and **(C)** ERα66 to GAPDH expression ratio shows measured increase and decrease in protein expression levels over 14 days (n = 2 slab gel western runs).

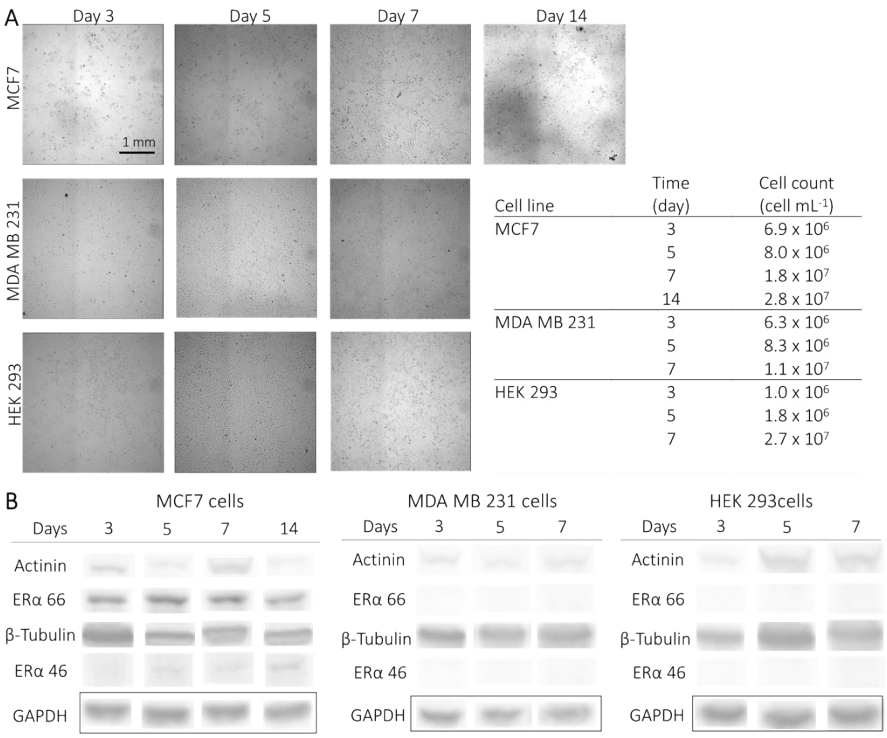

Cell line	Time (day)	Cell count (cell mL^{-1})
MCF7	3	6.9 x 10^6
	5	8.0 x 10^6
	7	1.8 x 10^7
	14	2.8 x 10^7
MDA MB 231	3	6.3 x 10^6
	5	8.3 x 10^6
	7	1.1 x 10^7
HEK 293	3	1.0 x 10^6
	5	1.8 x 10^6
	7	2.7 x 10^7

Figure S7. Comparison of cell confluency and ERα expression levels. **(A)** Bright-field images of MCF 7, MDA MB 231, and HEK 293 cells in corresponding culture days and counted cells per mL that are used to calculate confluency levels. **(B)** Identification of ERα isoforms in MCF 7, MDA MB 231, and HEK 293 cells by conventional slab gel Western blotting. Western blotting images were used in quantification of ERα isoforms in MCF 7 cells. No detectable signal was observed in MDA MB 231, and HEK 293 cells, as expected.

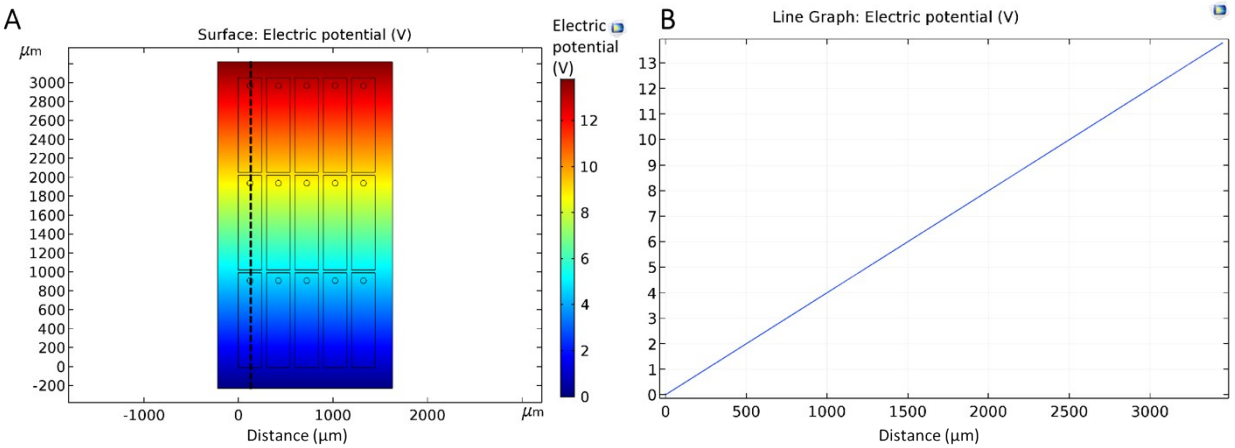

Figure S8. Finite element simulation of electric field distribution. Electric currents module of COMSOL Multiphysics software was operated by applying steady-state constant electric field through the matrix, where hydrogel and solution conductivities were set to 4304.0 μS m^{-1} estimated experimentally. **(A)** A section of microparticle array geometry and the cross section along which the electric field was simulated. **(B)** Electric field distribution in the section at dashed black line in panel A shows that microparticles do not disturb electric field distribution.